Dependence of Paranodal Junctional Gap Width on Transverse Bands

Jack Rosenbluth,[1]* Chris Petzold,[1] and Elior Peles[2]

[1]Department of Physiology & Neuroscience, New York University School of Medicine, New York, New York 10016
[2]Department of Molecular Cell Biology, Weizmann Institute of Science, Rehovot 76100, Israel

ABSTRACT

Mouse mutants with paranodal junctional (PNJ) defects display variable degrees of neurological impairment. In this study we compare control paranodes with those from three mouse mutants that differ with respect to a conspicuous PNJ component, the transverse bands (TBs). We hypothesize that TBs link the apposed junctional membranes together at a fixed distance and thereby determine the width of the junctional gap, which may in turn determine the extent to which nodal action currents can be short-circuited underneath the myelin sheath. Electron micrographs of aldehyde-fixed control PNJs, in which TBs are abundant, show a consistent junctional gap of ~3.5 nm. In *Caspr*-null PNJs, which lack TBs entirely, the gap is wider (~6–7 nm) and more variable. In *CST*-null PNJs, which have only occasional TBs, the mean PNJ gap width is comparable to that in *Caspr*-null mice. In the *shaking* mutant, in contrast, which has approximately 60% of the normal complement of TBs, mean PNJ gap width is not significantly different from that in controls. Correspondingly, *shaking* mice are much less impaired neurologically than either *Caspr*-null or *CST*-null mice. We conclude that in the absence or gross diminution of TBs, mean PNJ gap width increases significantly and suggest that this difference could underlie some of the neurological impairment seen in those mutants. Surprisingly, even in the absence of TBs, paranodes are to some extent maintained in their usual form, implying that in addition to TBs, other factors govern the formation and maintenance of overall paranodal structure. J. Comp. Neurol. 520:2774–2784, 2012.

INDEXING TERMS: dysmyelination; demyelination; multiple sclerosis; node of Ranvier; myelin

The paranodal axoglial junction (PNJ) of myelinated nerve fibers, first described by Robertson (1959), is unique in both structure and size. Its position just alongside the node of Ranvier suggests that it serves as a seal to prevent short-circuiting of nodal action currents underneath the myelin sheath, thereby facilitating saltatory conduction. Surprisingly, however, the junctional membranes are not fused together as they would be at a tight junction. Instead, they are separated by a distinct gap, several nm wide, representing a potential shunt pathway that could compromise the insulating properties of the myelin sheath (for review, see Rosenbluth, 2009).

The most distinctive component of the PNJ, the transverse bands (TBs) (Bargmann and Lindner, 1964; Andres, 1965), consists of a regular array of obliquely oriented ridges between the respective plasma membranes (Rosenbluth, 1995) comprised, at least in part, of the axonal Caspr/contactin complex and glial NF155 (Salzer et al., 2008). The function of the TBs is uncertain, but they are generally assumed to anchor the component plasma membranes to one another and to underlying cytoskeletal elements. We postulate that, in addition, the TBs serve to fix the width of the PNJ gap and that a patent gap of that width is of functional importance.

Genetically engineered mouse mutants affecting contactin (Boyle et al., 2001) or Caspr (Bhat et al., 2001; Gollan et al., 2003) display significant neurological defects. Previous studies have reported loss of TBs and focal widening of the PNJ gap in the central nervous system (CNS) and peripheral nervous system (PNS) of *Caspr*-null mice

Grant sponsor: National Institutes of Health; Grant numbers: NS 37475 (to J.R.) and NS50220 (to E.P.); Grant sponsor: the National Multiple Sclerosis Society; Grant number: RG 3618 (to J.R.); Grant sponsor: the Israeli Academy of Sciences (to E.P.).

*CORRESPONDENCE TO: J. Rosenbluth, M.D., Department of Physiology & Neuroscience, NYU School of Medicine, 550 First Avenue, New York, NY 10016. E-mail: rosenj03@med.nyu.edu

Received August 23, 2011; Revised January 31, 2012; Accepted March 7, 2012
DOI 10.1002/cne.23105
Published online March 20, 2012 in Wiley Online Library (wileyonlinelibrary.com)

(Bhat et al., 2001) and doubling of the gap width in the PNS of *contactin*-null mice (Boyle et al., 2001). These findings may reflect real differences in the separation of the junctional membranes, differences in the preparative methods used, or a combination of both.

In the present study, we have used consistent preparation and measurement methods to determine PNJ gap width in control mice and in three mutants that differ in various degrees with respect to their complement of TBs. Our results show significant increases in average gap width in mice lacking or grossly deficient in TBs. In contrast, in *shaking* mutant mice, which have marked CNS dysmyelination but large numbers of TBs (Mierzwa et al., 2010a), the PNJ gap width is not significantly different from that in controls. These results support the view that TBs determine the separation of the PNJ membranes, which may in turn affect the degree of nodal current shunting as one basis for the conduction abnormalities and neurological defects in the various mutant mice.

MATERIALS AND METHODS

Animals

Adult male or female mice ranging in age from 2.5 to 24 months were taken from our colonies in the NYUMC Berg animal facility. Three mutant lines, *Caspr*-null, *CST*-null, and *shaking* were used with normal littermates as controls.

The *CST*-null line was generated by gene targeting to replace the exon portions of the gene encoding the transmembrane domain and the 5′-PAPS binding motif with a neomycin-resistance cassette (Honke et al., 2002; Ishibashi et al., 2002). The mice used in this study were of mixed C57/black6 and 129 background.

The *Caspr*-null line was generated by gene targeting to replace a fragment of the first exon containing the initiator methionine and signal sequence with a neomycin-resistant gene (Gollan et al., 2003). The mice used in this study were on a mixed 129/ICR background. In both the *CST*-null and *Caspr*-null lines, heterozygotes, identified by polymerase chain reaction (PCR), were bred, resulting in homozygous mutant pups in one-fourth of the offspring.

The *shaking* mice came from a hybrid (C57Bl/6-129Sv) line developed from a spontaneous mutation tentatively identified as a *quaking* allele based on cross-breeding studies (Mierzwa et al., 2010a). In this case too, heterozygotes, identified by the results of prior matings, were bred, resulting in homozygous pups in one-fourth of the offspring. In all three mutants, the kinetic tremor characteristic of homozygotes appears by P14.

Mice were anesthetized with pentobarbital either alone or as a part of "Sleepaway," a mixture that also contains small amounts of propylene glycol and isopropanol, in accordance with our protocol approved by the NYUMC IACUC. In our experience these added ingredients have no apparent effect on nerve structure.

The heart was then exposed and the mice perfuse-fixed with 3% glutaraldehyde/2% paraformaldehyde in 0.1 M cacodylate buffer (pH 7.3–7.4). The spinal cord was removed and coronal slices cut through the cervical, midthoracic, and upper lumbar regions of three animals in each group. The aldehyde-fixed specimens were rinsed, postfixed in 2% OsO_4/1.5% ferricyanide/0.1 M cacodylate buffer (pH 7.3—7.4) for 2 hours, then rinsed and dehydrated in a graded series of methanol solutions, transferred to propylene oxide and embedded in Araldite.

Microscopy

Blocks were oriented for longitudinal sectioning of dorsal columns within their superficial third, i.e., through sensory fibers, not including the more centrally located efferent corticospinal tracts. The 1-μm sections were stained with alkaline toluidine blue for assessment of orientation and fixation by using a 60X planapochromatic objective lens. Then ~0.1-μm sections were cut, mounted on Formvar/carbon-coated copper mesh grids, stained with permanganate and alcoholic uranyl acetate, and surveyed in a JEOL JEM-1200 EX II microscope at 5,000–10,000X to locate nodal/paranodal regions of myelinated fibers. Paranodes were then photographed at 50,000X with a digital camera at a resolution of 2,116 dpi. All electron micrographs were taken at 80 kV.

Data analysis

Images of paranodal junctions were digitally enlarged and analyzed with ImageJ software (NIH) as follows. PNJ regions at which the apposed junctional membranes and intervening gap were cut normally and could be resolved clearly were selected randomly. A line tool was used for measuring the distance between the outermost dense components of the confronting junctional membranes. These measurements were stored in Excel files, and comparisons were made between data sets obtained from control and mutant mice. In view of possible differences among individual mice in each line, for example, related to variations in fixation or to variable penetrance of the gene defects, specimens from three mice were examined in each line. Measurements from each mouse were averaged, and those three means (meanL) were used as individual data points for that mouse line. Statistical comparisons among the four mouse lines were made by ANOVA followed by the post hoc Tukey test (SPSS, Chicago, IL). Statistical analyses comparing the four lines were carried out both including outliers and excluding outliers (i.e., values outside 1.5X the interquartile, Q1–Q3, range). A boxplot of all measurements, prepared with QI Macros

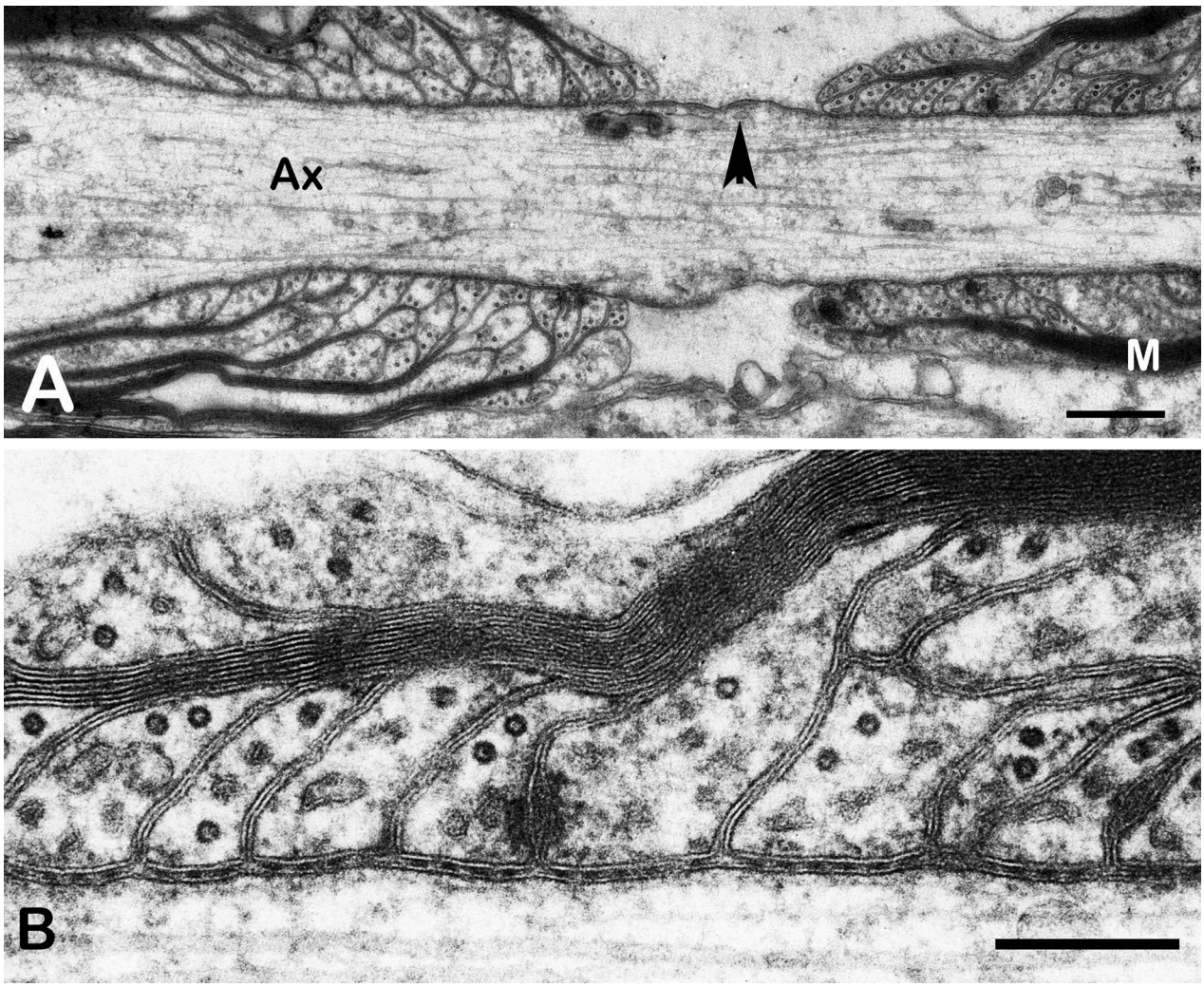

Figure 1. Control mouse spinal cord paranodes. **A:** Survey view showing control paranodes in which ~13 terminal loops are in contact with the axon (Ax) on each side of the node (arrowhead). Three to four loops are everted immediately adjacent to the node. M, compact myelin. **B:** Detail of survey view (upper right). The gap separating the junctional membranes contains transverse bands and is relatively consistent in width. Scale bar = 1 μm in A; 0.2 μm in B.

software (Denver, CO), provided the data on medians, quartiles, and outliers.

RESULTS

Control paranodes

Examination of electron micrographs shows the typical pattern of overlapping terminal loops apposed to the axon and indenting it slightly to produce a scalloped appearance. In the example shown in Figure 1A, ~13 loops contact the axon to form a paranodal junction ~4 μm long. Some of the loops do not reach the axon (Fig. 1B, upper right), and immediately adjacent to the node several loops are everted (Fig. 1A).

As shown in Figure 1B, the junctional membranes are clearly separated, and the junctional gap contains TBs. Measurement of the gap width (Table 1) shows that the averages among the three control animals vary within a narrow range (3.31–3.74 nm), with a mean of 3.53 ± 0.21 nm (SD). This figure is consistent with the generally accepted PNJ gap width of 2–4 nm. Presumably gap width at the site of the TBs is determined by the lengths of the molecules anchored in the axon and glial cell that bridge the gap and form the TBs. That length should be independent of external influences, e.g., osmotic forces, which under abnormal conditions can expand the gap width between TBs (Rosenbluth et al., 2009).

Caspr-null paranodes

Examination by electron microscopy (EM) shows a variety of abnormalities comparable to those in the Bhat et al. (2001) *Caspr*-null mutant. Many terminal loops face away from the axon or assemble into irregular formations

TABLE 1.

PNJ Gap Width (nm) in Control and Mutant Mouse Lines[1]

			Outliers IN				Outliers OUT					
ID No.	Line	No.	MeanL	SD	MeanG	SD	MeanL	SD	MeanG	SD	median	IQR
1	*Caspr-/-*	59	5.37	1.27			5.37	1.27				
2	*Caspr-/-*	23	7.75	4.22			6.08	1.12				
3	*Caspr-/-*	23	7.15	0.79			7.15	0.79				
		3			**6.76**	1.24			**6.20**	0.90		
		105									**6.12**	2.14
1	*CST-/-*	46	6.02	1.22			6.02	1.20				
2	*CST-/-*	13	6.16	1.06			6.16	1.06				
3	*CST-/-*	13	6.32	1.23			6.32	1.23				
		3			**6.17**	0.15			**6.17**	0.15		
		72									**6.01**	1.82
1	*shaking*	37	3.41	1.31			3.18	0.86				
2	*shaking*	19	4.64	1.23			4.29	0.73				
3	*shaking*	48	4.49	0.84			4.43	0.73				
		3			**4.18**	0.67			**3.96**	0.69		
		104									**3.98**	1.44
1	Control	55	3.54	1.01			3.53	0.80				
2	Control	29	3.31	0.82			3.31	0.82				
3	Control	29	3.74	0.63			3.74	0.63				
		3			**3.53**	0.21			**3.53**	0.21		
		113									**3.53**	0.96

[1]The multiple measurements made on each of the three animals in each mutant line were averaged to produce a mean for that animal (MeanL). Those three means were in turn averaged to produce the group mean (MeanG) for each mutant line (in bold face). Data are presented with outliers included (IN) and with outliers removed (OUT). Medians (in bold face) and interquartile ranges (IQR), as a measure of variability, are taken from analysis of the boxplot in Figure 5.

in which the loops abut each other instead of the axolemma (Fig. 2A). In addition, thin cellular processes sometimes insert themselves between the axolemma and a series of terminal loops (Fig. 2B). These intercalated processes may arise from the innermost layers of the myelin-forming cell itself and thus represent inner oligodendrocyte processes stripping off outer layers that are not anchored to the axolemma. In other cases (not shown), the intercalated processes contain bundles of intermediate filaments and thus represent astrocyte processes that have infiltrated the paranodal apparatus from outside the sheath. In the example shown in Figure 2B, a narrow gap separates the intercalated process from the axolemma, but no gap is apparent between the process and the terminal loops. These interrelations among the processes suggest that the intercalated process in this case arises from an oligodendrocyte, which typically forms tight junctions with other oligodendrocytes.

Despite these irregularities, the lateral edge of the myelin-forming *Caspr*-null oligodendrocyte to some extent still forms an overlapping series of terminal loops that indent the axon, and some *Caspr*-null terminal loops form junctions with the axolemma that look normal save for the absence of TBs (Fig. 3A). The width of the junctional gap is, however, more than 75% greater than control on average (6.76 $\pm$ 1.24 nm including outliers; 6.20 $\pm$ 0.90 nm without outliers; Table 1) and also more variable based on visual inspection (Fig. 3A–C) and comparison of standard deviations and interquartile ranges (Table 1 and Fig. 5).

CST-null paranodes

Examination of *CST*-null CNS fibers also shows paranodal irregularity, eversion of terminal loops, stripping of loops by cellular processes, as reported previously (Dupree et al.1998; Marcus et al., 2006), and a marked dearth of TBs (Fig. 4B, C). PNJ gap width among the three animals in this group is again significantly larger than that at control PNJs, varying from 6.02 to 6.32 nm (mean: 6.17 $\pm$ 0.15 nm; Table 1).

shaking mouse paranodes

PNJs in the *shaking* CNS are distinct from those in the *Caspr*-null and *CST*-null specimens in that TBs are to a large extent present (~60% of control; Mierzwa et al., 2010a), as shown in Figure 4A. This mutant is of interest also because despite extensive abnormalities in its CNS myelin, including a considerable degree of demyelination, the mice are much less severely affected neurologically than the mutants that have a gross deficiency of transverse bands.

Measurement of the PNJ gap in the *shaking* mouse CNS yielded an average width that varied from 3.41 to 4.49 nm among the three animals (3.18 to 3.43 nm excluding outliers) with an overall mean of 4.18 $\pm$ 0.67

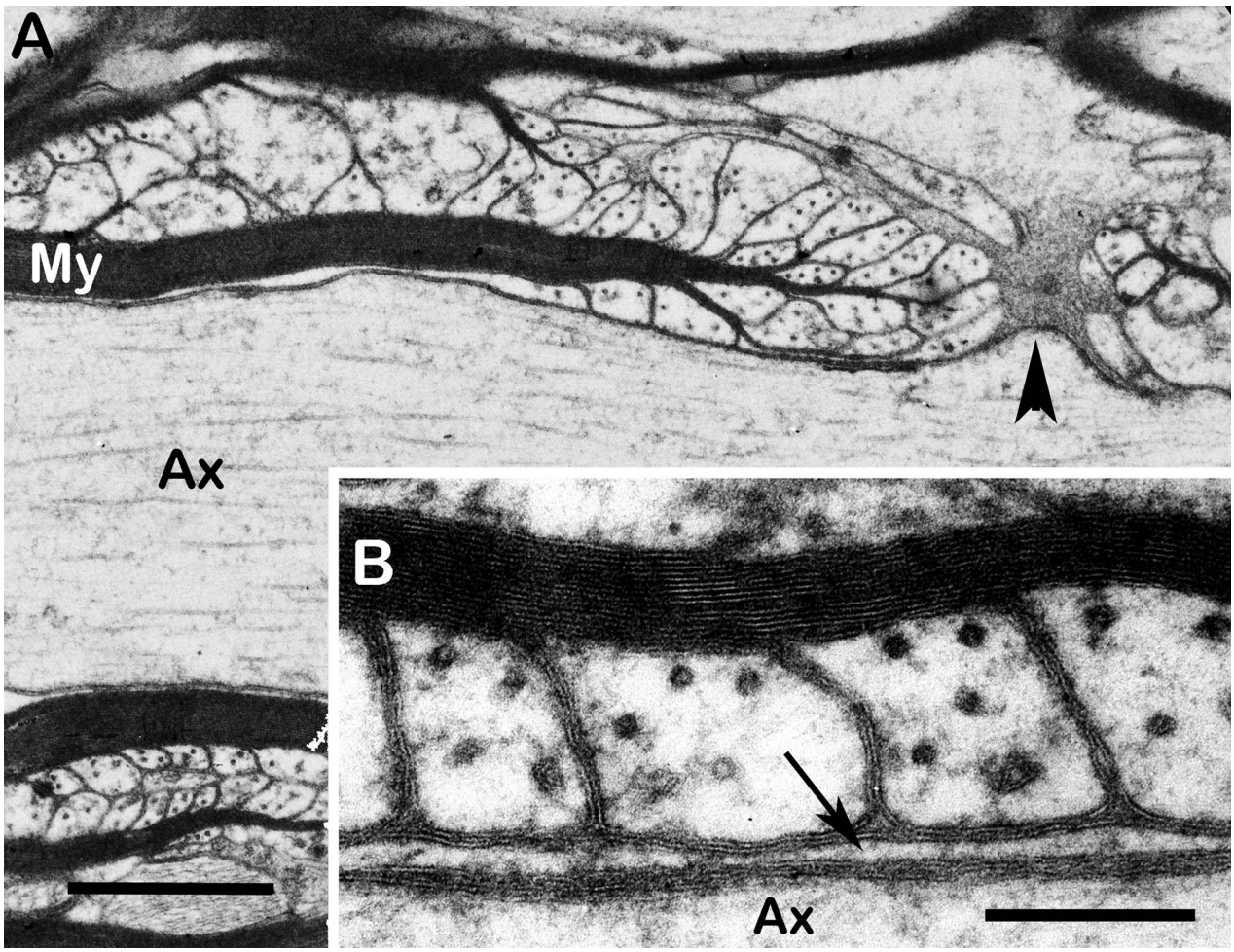

Figure 2. *Caspr*-null spinal cord paranodes. **A:** Survey view showing an axon (Ax) covered by compact myelin (My), which forms a complex paranodal apparatus adjacent to the node of Ranvier (arrowhead). The node is surrounded by an amorphous perinodal extracellular matrix. Note that of the myriad paranodal terminal loops, only four make contact with the axolemma. The others end on one another or face away from the axon. **B:** Example showing a succession of normal-looking terminal loops ending against a thin cytoplasmic sheet (arrow) interposed between them and the axon (Ax) below. The intercalated process is probably oligodendroglial (see text). Scale bar = 1 μm in A; 0.2 μm in B.

nm (3.96 ± 0.69 nm), which, although apparently larger than the control values, does not differ significantly from them (Tables 1 and 2).

Statistical analysis

Comparison of the four groups of mice by one-way ANOVA, using the three meanL values for each line (Table 1), reveals significant differences among the respective mouse lines ($P = 0.001$). We then carried out post-ANOVA comparisons of the four groups. Comparison of the meanL values among the mouse lines ($n = 3$ per line) using Tukey's post hoc test showed that PNJ gap width in the *Caspr*-null and *CST*-null lines was significantly larger than that in either the control or *shaking* line. The *Caspr*-null and *CST*-null gap widths were not significantly different from each other, and the control and *shaking* gap widths were also not significantly different from each other (Tables 1 and 2).

A boxplot comparing mutant and control CNS gap widths is shown in Figure 5, and the analysis is included in Table 1. Median gap widths for *Caspr*-null and *CST*-null are ~6.12 and 6.01 nm, respectively, and for *shaking* and control they are ~3.98 and 3.53 nm, respectively. The interquartile range is least in the control group (0.96 nm), ~2X control in the *Caspr*-null and *CST*-null groups (2.14 and 1.82 nm, respectively), and ~1.5X control in the *shaking* group (1.44 nm). By this measure, the variability in gap width is least in the control mice, which have a full complement of TBs, and most in the *Caspr*-null mice, which lack TBs entirely. Similarly, comparison of the meanG results (Table 1) shows a much larger SD in the *Caspr*-null group than in control, whether outliers are

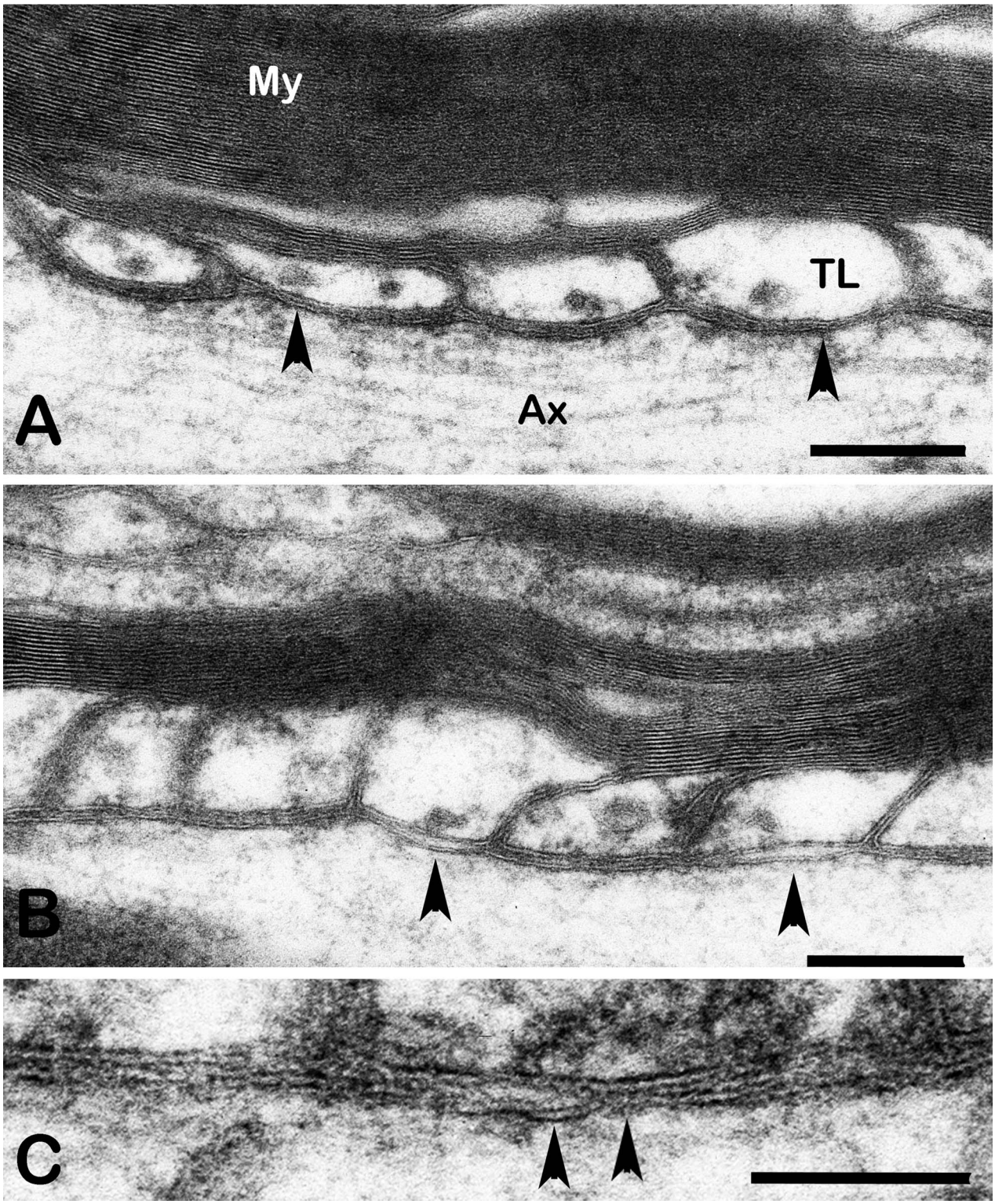

Figure 3. *Caspr*-null spinal cord paranodes. **A:** Terminal loops (TL) indent the axon (Ax), resulting in scalloping of the axon membrane. Arrowheads show two regions in which the gap between the terminal loop membrane and the axolemma cannot be resolved. My, compact myelin. **B:** Arrowheads indicate two regions at which the gap between the terminal loop and axolemma is widened in contrast to the much closer apposition at the intervening terminal loop. **C:** Left arrowhead indicates a region at which the gap between the terminal loop membrane (above) and the axolemma (below) is widened immediately adjacent to a region (right arrowhead) at which the gap cannot be resolved. Scale bar = 0.2 μm in A, B; 0.1 μm in C.

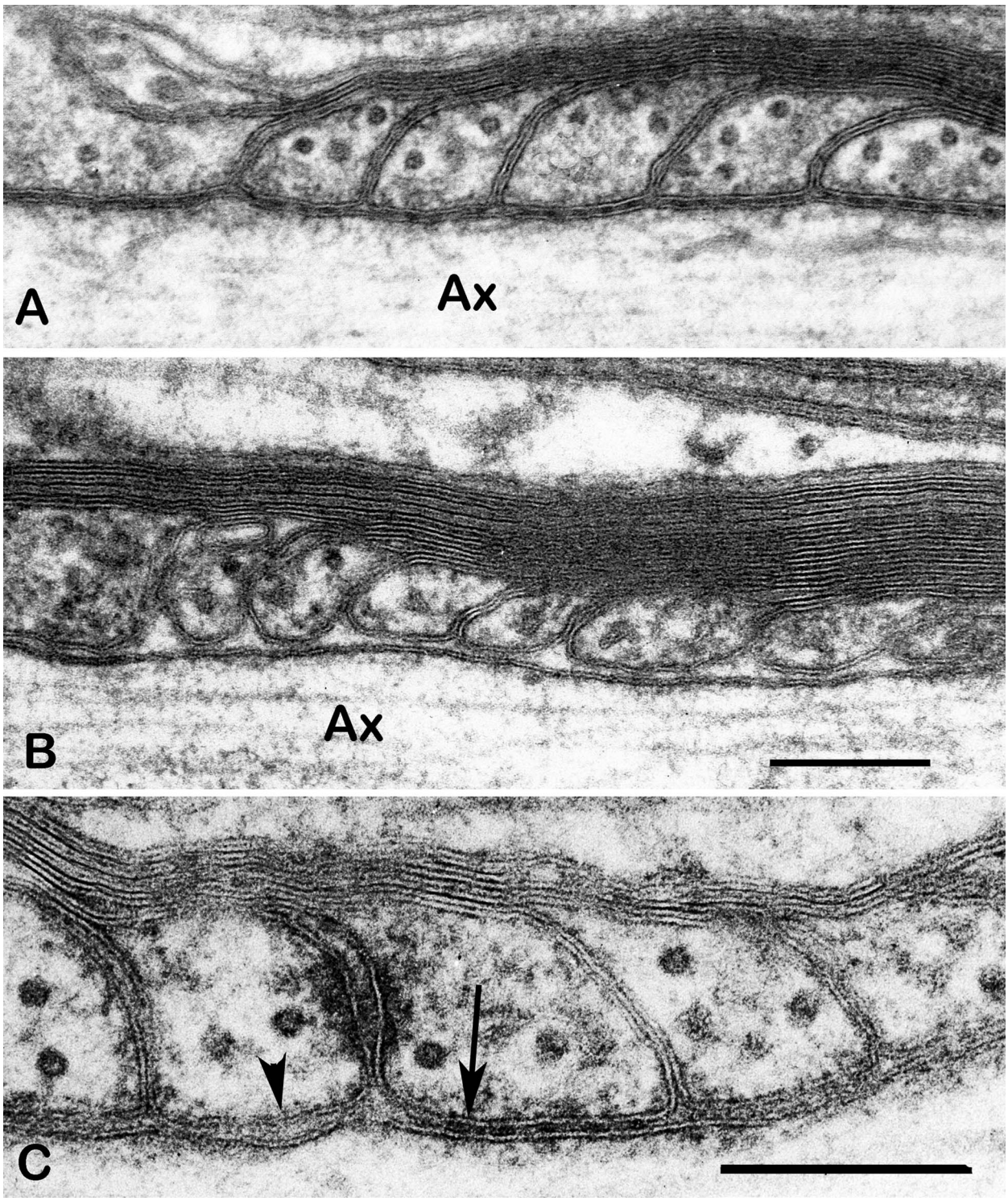

Figure 4. *shaking* and *CST*-null spinal cord paranodes. **A:** *shaking*. Paranodal loops adjoin the axon at a consistent separation, indenting the axon slightly. Transverse bands are visible at each loop. No large extracellular spaces are present between the loops or between them and the axolemma. **B:** *CST*-null. Transverse bands, which are seen occasionally in this mutant, are not visible in this image. The PNJ gap between the terminal loops and the axon (Ax) is variable in width and larger than that in controls on average (see Fig. 5). The edges of the loops tend to peel away from the axolemma, resulting in enlarged triangular spaces between the adjacent loops. **C:** *CST*-null. In one region of this PNJ (arrow), transverse bands are present. In an adjacent region (arrowhead), where they are absent, the confronting membranes are more variably and more widely separated. Scale bar = 0.2 μm in B (also applies to A) and C.

TABLE 2.

Post-ANOVA Statistical Analyses of Paranodal Junctional Gap Widths[1]

	P values		
	Post-ANOVA Tukey		
	Outliers IN	Outliers OUT	Significance
Caspr-null vs. *CST*-null	0.750	1.000	ns
Caspr-null vs. *shaking*	**0.010**	**0.006**	**S**
Caspr-null vs. control	**0.002**	**0.002**	**S**
CST-null vs. *shaking*	**0.038**	**0.007**	**S**
CST-null vs. control	**0.009**	**0.002**	**S**
shaking vs. control	0.693	0.790	ns

[1]Pairs of mouse lines were compared based on the three "meanL" entries for each line (Table 1). Data sets with outliers included (IN) and with outliers removed (OUT) were tested separately and yielded comparable results. Tukey post hoc tests of pairs showed no significant difference between the *Caspr*-null and *CST*-null results or between the *shaking* and control results. In contrast, comparison of the *Caspr*-null or *CST*-null results with either the *shaking* or control results did show a significant difference (in bold face).

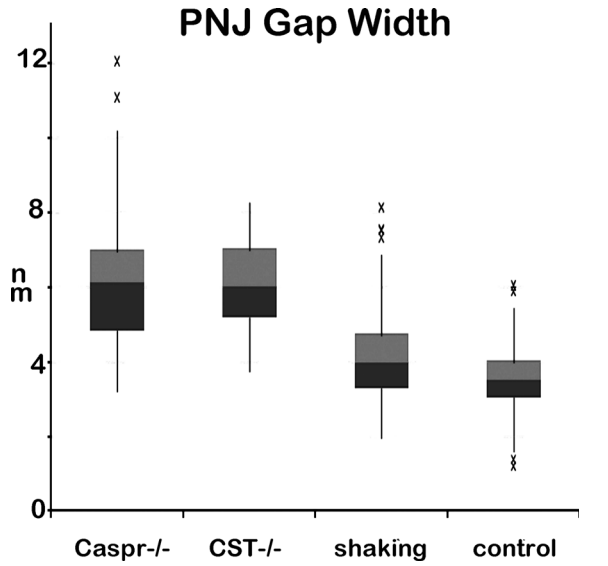

Figure 5. Boxplot of PNJ gap widths. The ends of the whiskers are the greater of the maximum (minimum) value or 1.5X the interquartile (IQ) distance, i.e., the distance from the first to the third quartile marked by the top and bottom of each box. Outliers are indicated by x. Two additional *Caspr*-null outliers (19.5 and 19.9 nm) are off the chart. Control and *shaking* medians are <4 nm. *Caspr*-null and *CST*-null medians are >6 nm. The interquartile range (IQR) for the *Caspr*-null and *CST*-null mice is ~2X that for the control mice; *shaking* IQR is intermediate.

included (~6X) or not (~4–5X). These results are consistent with the visual impression obtained from electron micrographs, e.g., Figure 4C, where PNJ gap width in the region displaying TBs is not only narrower but also more consistent than that in the adjacent region that lacks TBs at a *CST*-null paranode.

DISCUSSION

The principal findings in this study are as follows:

1. CNS paranodes that have no TBs (*Caspr*-null) or few TBs (*CST*-null) nevertheless display many terminal loops forming the typical overlapping series against the axolemma.
2. In the *Caspr*-null and *CST*-null mice these loops form junctions at which the axonal and glial plasma membranes are separated by a gap significantly wider on average than that at control PNJs (>6 nm versus ~3.5 nm).
3. PNJ gap width in control mice varies within a narrow range compared with *Caspr*-null mice.
4. The PNJ gap width in the *shaking* mutant, which contains diminished, but still substantial numbers of TBs, is close to that in controls and significantly smaller than that in both the *Caspr*-null and the *CST*-null mice.

Significance of the junctional gap

Early drawings of myelinated nerve fibers depicted the myelin sheath as a tight-fitting amorphous sleeve that tapered as it approached the node (Ranvier, 1879). The presumption by electrophysiologists subsequently was that inward current at the node flowed longitudinally through the axon and exited at the adjacent nodes a distance away because of the high resistance and low capacitance of the myelin sheath covering the intervening internodal axon, resulting in efficient, high-speed saltatory conduction (Huxley and Staempfli, 1949). It was therefore surprising to find that the paranodal myelin sheath does in fact *not* form a tight junction with the axon but rather is separated from it by a distinct gap. Single ex vivo fiber studies also show a current flow from internode to node following the action potential, attributed to discharge of internodal capacitance and thought to travel under or through the myelin sheath (Barrett and Barrett, 1982). Recent tracer studies do in fact demonstrate an open pathway for dextran tracers through the living paranode, probably corresponding to the helical space between successive turns of the lateral edge of the myelin sheath as it winds around the axon (Mierzwa et al., 2010b; Shroff et al., 2011). In addition, the PNJ gap itself may constitute a patent pathway for current flow through the paranode, which, however, would still represent only a small proportion of the total current generated at each node, because of the narrow width, and thus high resistance, of the gap, and would therefore not compromise saltatory conduction significantly.

Posssible functions of these pathways through the paranode have been reviewed (Rosenbluth, 2009). One of

these involves the fast, voltage-gated K^+ channels that lie underneath the myelin sheath in the juxtaparanodal (JP) region (Wang et al., 1993), along the helical inner mesaxon in the internode, and facing the inner portions of Schmidt–Lanterman clefts in peripheral nerves (Arroyo et al., 1999) Mouse mutants that lack these K^+ channel accumulations display seizures and conduction abnormalities (Chiu et al., 1999). In the developing CNS, JP K^+ channels are active during signal propagation (Vabnick et al., 1999). Further evidence that JP K^+ channels play a role in conduction came more recently from a study of small-caliber fibers in the CNS (Devaux and Gow, 2008), which showed that K^+ channel blockers change the wave-form of the CAP in the thinnest fibers, although they have minimal effect on the largest CNS fibers, as would be expected because the paranodal pathways to the JP K^+ channels are decidedly longer in the case of thickly myelinated fibers, which have longer paranodes, and their conductance is accordingly smaller. Thus, there is evidence that JP K^+ channels play a significant role in modulating nodal electrical activity in some fibers under normal conditions.

They may also affect conduction under pathological conditions that increase conductance through the paranode. In multiple sclerosis, e.g., demyelination and remyelination result in the formation of shadow plaques in which myelin is thinner than normal. Paranodes are therefore shorter than normal, thus more permeable to tracers (Shroff et al. 2011), and undoubtedly more conductive as well to currents that could activate JP K^+ channels and might thereby reduce the amplitude of the inward currents at adjacent nodes. In addition, even before demyelination, the early inflammatory process in multiple sclerosis could result in the release of proteases in the vicinity of PNJs, which could lyse TBs, resulting in disjunction of paranodal loops and widening of the PNJ cleft. Thus, conduction could be compromised by this subtle change early in the process, well before frank demyelination occurs.

The observations in the present report were all made on CNS PNJs, but the same considerations apply to peripheral nerves as well. Previous studies have shown widening of the PNJ gap in peripheral nerves of mutants lacking TBs (Bhat et al., 2001; Boyle et al., 2001). Preliminary studies have also shown widening of the PNJ gap in *Caspr*-null and *CST*-null sciatic nerves to approximately the same extent as that seen in the CNS of these mutants, but no apparent widening in *shaking* sciatic nerves (Rosenbluth et al., unpublished data).

The real size of the PNJ gap

Previous EM studies of nervous tissue have led to the impression that membranes in the CNS stabilize at a separation of 10–20 nm even in perfusion-fixed specimens. The evidence from more recent diffusion studies in live CNS indicates, however, that the space in the living tissue is much larger, ~38–64 nm (Thorne and Nicholson, 2006). The difference has been attributed to anoxia and tissue swelling during fixation, but the change in the ionic milieu of the confronting membranes associated with fixation and dehydration might equally well account for a change in the distance at which they stabilize.

In any case, the apparent PNJ gap width in fixed tissue may be equally inaccurate for the same reasons, except in cases in which TBs interconnect the respective membranes. There the space is probably determined by the lengths of the external domains of the axonal Caspr/contactin complex and the glial NF155 molecule and the way in which they bind to each other (Gollan et al. 2003). Other molecules may also contribute to structural interaction between PNJ membranes (Jarjour et al., 2008).

In addition to the effects of fixation, the methods used for measurement may also affect apparent gap width. In EM tomograms of normal aldehyde-fixed specimens (Sosinsky et al., 2005; Nans et al., 2011), PNJ gap width is reported to be as large as 7.4 nm. The difference from the dimensions obtained from standard transmission EMs could arise from minor undulations of the confronting membranes that superimpose within the thickness of a 0.1-μm section to reduce the apparent width of the gap.

Although TBs may determine PNJ gap width with reasonable accuracy when they are present, tracer studies and diffusion kinetics may be needed to define the membrane separation at PNJs lacking TBs. EM studies of rapidly frozen unfixed specimens might also more accurately indicate the true separation of the membranes, but these too are subject to artifacts.

The data we present here are useful in that the specimens have all been prepared in the same manner and examined with the same electron microscope at the same magnification. Most important, because there is some subjectivity in deciding exactly where to begin and end each measurement, ours were made in the same laboratory in a consistent manner. Thus, although the absolute distances found may differ from those in the living state, the data obtained from the various mutants examined can still be used to compare them meaningfully.

Previous mathematical models of myelinated nerve fiber conduction allowed for variations in such parameters as node length and myelin thickness but did not take into account variations in PNJ gap width. More recently, variations in PNJ gap width have been considered as well (see Fig. 4 in Poliak and Peles, 2003, based on the Hines and Shrager, 1991, model, and Vabnick et al., 1999). The data presented in this study may thus be useful in refining such models and allowing more accurate predictions to

be made about conduction in myelinated nerve fibers with defects in TBs.

Axolemmal domain organization

To what extent maintenance of sodium channels at the node of Ranvier depends on node-specific or paranode-specific mechanisms or both has long been a subject of controversy (Susuki and Rasband, 2008; Zonta et al., 2008; Rosenbluth, 2009; Feinberg et al., 2010). If node-specific mechanisms alone were sufficient to specify nodal domain structure and confine the nodal sodium channels to that domain, paranodal abnormalities should have no effect on nodal structure. In comparing *Caspr*-null mice with normals, the mutant paranodes are certainly abnormal in form, but nodal abnormalities are also present. Specifically, "The distribution of the Na channels is wider and more diffuse at the nodes of mutant mice. . ." (Bhat et al., 2001). Similarly, in *CGT*-null (Rosenbluth et al., 2003) and *CST*-null mice (Dupree et al., 1998), which display loss or marked diminution of TBs, paranodes display gross abnormalities, and in both cases the nodes gradually become larger and more irregular in shape, with corresponding abnormalities in capacitance and sodium channel distribution, resulting in progressive conduction failure (Rosenbluth, 2009; Mierzwa et al., 2010a).

Even before these slow, progressive changes occur, fewer paranodal loops adjoin the axolemma in the *Caspr*-null and *CST*-null mice. Shortening of paranodes would be expected to increase conductance through the paranodal pathway between the node and juxtaparanode, resulting in a proportionate increase in the amount of nodal action current shunted underneath the myelin sheath, a corresponding diminution in passive current density at the adjacent nodes, and an increased possibility that JP K^+ channels would be activated and in turn reduce total nodal inward current. Lengthening of the nodal domain would increase its capacitance, further slowing conduction velocity. Thus, the domain abnormalities in mutant nerves with TB deficiency can have significant physiological consequences mediated by changes in paranodes as well as nodes.

ACKNOWLEDGMENTS

The authors thank Moses V. Chao and Juan Carlos Arevalo, Skirball Institute, NYU School of Medicine, for their advice and assistance in making the *shaking* mice available.

LITERATURE CITED

Andres KH. 1965. Uber die Feinstruktur besonderer Einrichtungenin markhaltigen Nervenfasern des Kleinhirns der Ratte. Z Zellforsch 65:701–712.

Arroyo EJ, Xu YT, Zhou L, Messing A, Peles E, Chiu SY, Scherer SS. 1999. Myelinating Schwann cells determine the internodal localization of Kv1.1, Kv1.2, Kvbeta2, and Caspr. J Neurocytol 28:333–347.

Bargmann W, Lindner E. 1964. Uber den Feinbau des Nebennierenmarkes des Igels (*Erinaceous europaeus* L), Z Zellforsch 64:868–912.

Barrett EF, Barrett JN. 1982. Intracellular recording from vertebrate myelinated axons: mechanism of the depolarizing afterpotential. J Physiol 323:117–144.

Bhat MA, Rios JC, Lu Y, Garcia-Fresco GP, Ching W, St Martin M, Li J, Einheber S, Chesler M, Rosenbluth J, Salzer JL, Bellen HJ. 2001. Axon-glia interactions and the domain organization of myelinated axons requires neurexin IV/Caspr/Paranodin. Neuron 30:369–383.

Boyle ME, Berglund EO, Murai KK, Weber L, Peles E, Ranscht B. 2001. Contactin orchestrates assembly of the septate-like junctions at the paranode in myelinated peripheral nerve. Neuron 30:385–397.

Chiu SY, Zhou L, Zhang C-L, Messing A. 1999. Analysis of potassium channel functions in mammalian axons by gene knockouts. J Neurocytol 28:349–364.

Devaux J, Gow A. 2008. Tight junctions potentiate the insulative properties of small CNS myelinated axons. J Cell Biol 183:909–921.

Dupree JL, Coetzee T, Blight A, Suzuki K, Popko B. 1998. Myelin galactolipids are essential for proper node of Ranvier formation in the CNS. J Neurosci 18:1642–1649.

Feinberg K, Eshed-Eisenbach Y, Frechter S, Amor V, Salomon D, Sabanay H, Dupree JL, Grumet M, Brophy PJ, Shrager P, Peles E. 2010. A glial signal consisting of gliomedin and NrCAM clusters axonal Na+ channels during their formation of nodes of Ranvier. Neuron 65:490–502.

Gollan L, Salomon D, Salzer JL, Peles E. 2003. Caspr regulates the processing of contactin and inhibits its binding to neurofascin. J Cell Biol 163:1213–1218.

Hines M, Shrager P. 1991. A computational test of the requirements for conduction in demyelinated axons. Restor Neurol Neurosci 3:81–93.

Honke K, Hirahara Y, Dupree J, Suzuki K, Popko B, Fukushima K, Fukushima J, Nagasawa T, Yoshida N, Wada Y, Taniguchi N. 2002. Paranodal junction formation and spermatogenesis require sulfoglycolipids. Proc Natl Acad Sci U S A 99: 4227–4232.

Huxley AF, Staempfli R. 1949. Evidence for saltatory conduction in peripheral myelinated nerve fibers. J Physiol 108: 315–339.

Ishibashi T, Dupree JL, Ikenaka K, Hirahara Y, Honke K, Peles E, Popko B, Suzuki K, Nishino H, Baba H. 2002. A myelin galactolipid, sulfatide, is essential for maintenance of ion channels on myelinated axon but not essential for initial cluster formation. J Neurosci 22:6507–6514.

Jarjour AA, Bull SJ, Almasieh M, Rajasekharan S, Baker KA, Mui J, Antel JP, Di Polo A, Kennedy TE. 2008. Maintenance of axo-oligodendroglial paranodal junctions requires DCC and netrin-1. J Neurosci 28:11003–11014.

Marcus J, Honigbaum S, Shroff S, Honke K, Rosenbluth J, Dupree JL. 2006. Sulfatide is essential for the maintenance of CNS myelin and axon structure. Glia 53: 372–381.

Mierzwa A, Arevalo JC, Schiff R, Chao M, Rosenbluth J. 2010a. Role of transverse bands in maintaining paranodal structure and axolemmal domain organization in myelinated nerve fibers: effect on longevity in dysmyelinated mutant mice. J Comp Neurol 518:2841–2853.

Mierzwa A, Shroff S, Rosenbluth J. 2010b. Permeability of the paranodal junction of myelinated nerve fibers. J Neurosci 30:15962–15968.

Nans A, Einheber S, Salzer J, Stokes D. 2011. Electron tomography of paranodal septate-like junctions and the associated axonal and glial cytoskeletons in the central nervous system. J Neurosci Res 89:310–319.

Poliak S, Peles E. 2003. The local differentiation of myelinated axons at nodes of Ranvier. Nat Rev Neurosci 4:968–980.

Ranvier L-A. 1878. Leçons sur l'histologie du système nerveux. Paris: Weber.

Robertson JD. 1959. Preliminary observations on the ultrastructure of nodes of Ranvier. Z Zellforsch 50:553–560.

Rosenbluth J. 1995. Glial membranes and axoglial junctions. In: Kettenmann H, Ransom B, editors. Neuroglia. New York: Oxford University Press. pp 613–633.

Rosenbluth J. 2009. Multiple functions of the paranodal junction of myelinated nerve fibers. J Neurosci Res 87:3250–3258.

Rosenbluth J, Dupree JL, Popko B. 2003. Nodal sodium channel domain integrity depends on the conformation of the paranodal junction, not on the presence of transverse bands. Glia 41:318–325.

Rosenbluth J, Schiff R, Lam P. 2009. Effects of osmolality on PLP-null myelin structure: implications re axon damage. Brain Res 1253:191–197.

Salzer JL, Brophy PJ, Peles E. 2008. Molecular domains of myelinated axons in the peripheral nervous system. Glia 56: 1532–1540.

Shroff S, Mierzwa A, Scherer SS, Peles E, Arevalo JC, Chao MV, Rosenbluth J. 2011. Paranodal permeability in myelin mutants. Glia 59:1447–1457.

Sosinsky GE, Deerinck TJ, Greco R, Buitenhuys CH, Bartol TM, Ellisman MH. 2005. Development of a model for microphysiological simulations: small nodes of ranvier from peripheral nerves of mice reconstructed by electron tomography. Neuroinformatics 3:133–162.

Susuki K.Rasband MN. 2008. Molecular mechanisms of node of Ranvier formation. Curr Opin Cell Biol 20:616–623.

Thorne RG, Nicholson C. 2006. In vivo diffusion analysis with quantum dots and dextrans predicts the width of brain extracellular space. Proc Natl Acad Sci USA 103:5567–5572.

Vabnick I, Trimmer JS, Schwarz TL, Levinson SR, Risal D, Shrager P. 1999. Dynamic potassium channel distributions during axonal development prevent aberrant firing patterns. J Neurosci 19:747–758.

Wang H, Kunkel DD, Martin TM, Schwartzkroin PA, Tempel BL. 1993. Heteromultimeric K+ channels in terminal and juxtaparanodal regions of axons. Nature 365:75–79.

Zonta B, Tait S, Melrose S, Anderson H, Harroch S, Higginson J, Sherman DL, Brophy PJ. 2008. Glial and neuronal isoforms of neurofascin have distinct roles in the assembly of nodes of Ranvier in the central nervous system.. J Cell Biol 181:1169–1177.